Solid Freeform Fabrication 2023: Proceedings of the 34th Annual International Solid Freeform Fabrication Symposium – An Additive Manufacturing Conference
Reviewed Paper

ON PROCESS STABILITY IN WAAM-CMT OF ALUMINUM ALLOYS

Austen Thien*†, Kathryn M. Kelly*, Caroline E. Massey*, Christopher J. Saldana*

**George W. Woodruff School of Mechanical Engineeirng*
Georgia Institute of Technology
801 Ferst Drive, Atlanta, GA 30332, USA
†athien6@gatech.edu

Abstract

Wire-arc additive manufacturing (WAAM) has become a cost-efficient metal additive manufacturing process. However, depositing aluminum with WAAM is challenging due to its sensitivity to heat input (linear energy density), which can cause undesirable surface topology waviness if not controlled. Thus, a process window is needed that can produce stable geometry and deposition conditions while minimizing production times. In this study, 5183 aluminum alloy wire is used to deposit 10-layer walls with varying wire feed speeds (WFS) and traverse speeds (TS) (at a constant WFS/TS ratio) and varying interpass temperature (IPT). In-situ process data consisting of optical contact-tip-workpiece-distance (CTWD) and current/voltage measurements are collected to determine process condition stability throughout the build. Part geometry is measured using a 3D scanner and build porosity is characterized via digital X-ray. A process window is identified that produces stable surface topology and process conditions at a minimal production time.

Introduction

Additive manufacturing (AM) has made way for incredible advancements in the field of engineering with a variety of materials. Additive manufacturing allows for significant design freedom of both metal and polymer components. One of the methods by which parts are created using AM is through wire-arc additive manufacturing (WAAM), where a solid wire material is fed through the system and an electric arc is used as the heat source to deposit the material [1]. Currently, WAAM is most praised for its high deposition rates of material that are faster than any other currently existing AM method [1, 2]. By utilizing different welding techniques, different results can be obtained. For example, gas metal arc welding (GMAW) is a traditional welding technique that features a constant liquid metal pool [1]. However, a more advanced welding process known as cold metal transfer (CMT) has been developed specifically for AM. This process incorporates control over the electrode wire tip in a steady back and forth motion to control the droplet transfer and therefore limit the heat input of the welding process [1]. By doing so, it produces both a spatter-free weld and has noticeably less heat input and lower energy than compared with other GMAW welding modes [3].

Aluminum is often referred to as the ideal material for applications to transportation, electrical, machinery, construction, and many more fields [4]. CMT is especially useful for aluminum prints due to the material characteristics of aluminum. It's been proven that the low thermal input, yet high wire melting coefficient is beneficial to aluminum's sensitivities to heat, making CMT a highly effective welding process when compared to GMAW or regular metal inert gas (MIG) welding [5]. Unfortunately, there have been recurring problems with aluminum welding due to its material properties, one of which being porosity formation [4]. Porosity is caused by a moisture build-up in the shielding gas or the wire from the chemical reactions in

welding that release hydrogen as a byproduct [6, 7]. In some cases, post-processing can be used to reduce porosity, but also removes the appeal of the reduced welding time associated with aluminum CMT. While CMT has been found to produce a less porous result than GMAW and pulsed-GMAW, it does not fully eliminate the porosity in a part [7].

This paper aims to describe a further reduction in the porosity generated by the CMT AM process. Because the process of welding aluminum is incredibly heat-dependent, the following study analyzes the dependency of a WAAM build on the temperatures present during the build. A previous study found that using a deposition strategy with a lower thermal exposure of the alloy creates a more homogenous microstructure [8], but the hypothesis proposed is that a higher thermal exposure will cause the aluminum to melt into itself more effectively. This study will also analyze the effects of altering the wire feed speed (WFS) and traverse speed (TS), while keeping the WFS to TS ratio (WFS:TS) relatively constant. This value was picked from previously performed experimentation [9]. The porosity values will be recorded to find the optimal parameters to perform aluminum CMT welding with minimal or no porosity left behind.

Main Method

A. WAAM CMT Cell

The WAAM cell used for this work can be seen below in Figure 1a. The Fronius TPS/I 400 power supply is connected to a Robacta CMT drive on the welding torch which is in turn integrated into a Fanuc LR Mate 200iD/7L. The build plate substrate is fixed in a vice on a welding table. The optical camera used to view the contact tip to workpiece distance (CTWD) is mounted to the torch as shown in Figure 1b.

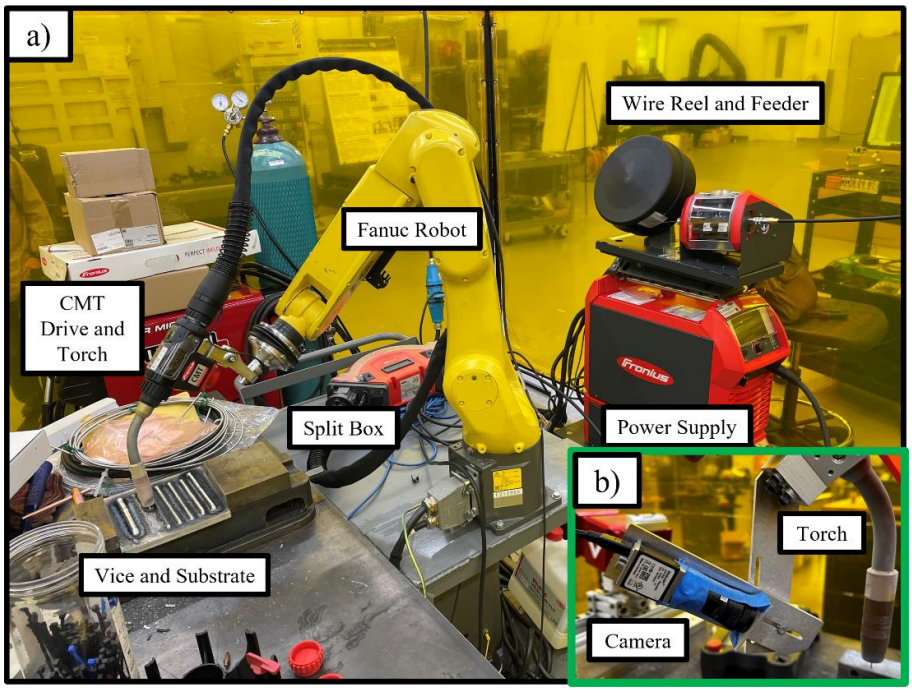

Figure 1: a) WAAM CMT cell; b) optical camera mounting location

The deposition material used for these experiments is 5183 aluminum alloy in the form of 1.2 mm diameter wire. The substrate used in these experiments is 6061 aluminum alloy and has dimensions of 12.5 x 203.2 x 50.8 mm. The chemical composition of both the wire and the substrate can be found below in Table 1.

Table 1: Chemical composition of wire and substrate

Component	**Composition %**											
6061 Substrate	*Al*	*Cr*	*Cu*	*Fe*	*Mg*	*Mn*	*Ni*	*Si*	*Ti*	*Zn*	*Zr*	*Other*
	95.1-98.2	0.4-0.8	0.05-0.4	0-0.7	0.8-1.2	0-0.15	0-0.05	0.4-0.8	0-0.15	0-0.25	0-0.25	0.15
5183 Wire	*Al*	*Cr*	*Cu*	*Fe*	*Mg*	*Mn*	*Be*	*Si*	*Ti*	*Zn*	*Other*	
	Bal.	0.05-0.25	0.1	0.4	4.3-5.2	0.5-1.0	0.0003	0.4	0.15	0.25	0.15	

B. Experimental Method

There are several process parameters varied in this study that influence the resulting deposition geometry, process conditions, and part quality. The wire feed speed (WFS) is the rate at which wire is being fed into the melt pool of the deposition process, the traverse speed (TS) is how fast the welding torch moves during the deposition process, and the inter-pass temperature (IPT) is the temperature to which the part must cool down after a layer is deposited and before another layer can be deposited.

The combination of WFS and TS controls the material input rate and the heat input rate since the TS controls how long the electrical arc heat source spends in a given location along the deposition toolpath and the WFS controls the current used in the deposition process. The material input rate can be represented as the WFS/TS ratio. The heat input rate is typically represented as the linear energy density (LED). The IPT dictates the cooling rate for each layer of the deposition process. Additionally, the TS and IPT control the overall deposition production time for the build.

Based on previously reported findings, the WFS and TS values are varied such that a WFS/TS ratio of ~9.2 is used and the material rate is approximately the same for each deposition [9]. Additionally, IPT values of 50, 75, and 100 ºC are chosen based on previous research in WAAM CMT for aluminum alloys [5-9]. The specific parameter sets used in each experiment can be seen below in Table 2.

Table 2: Process parameter values

Experiment	WFS (m/min)	TS (m/min)	WFS/TS	IPT (ºC)
1	4.7	0.51	9.25	50
2	5.33	0.58	9.13	50
3	6.1	0.66	9.23	50
4	4.7	0.51	9.25	75
5	5.33	0.58	9.13	75
6	6.1	0.66	9.23	75
7	4.7	0.51	9.25	100
8	5.33	0.58	9.13	100
9	6.1	0.66	9.23	100

The path planning approach used for these experiments follows general heuristics about additive manufacturing, where the deposition direction is rotated by 180º every layer, as shown below in Figure 2a, so that the height disparities at the transient start and stop points of each layer are distributed evenly. Additionally, due to the naturally low heat input of the CMT process, the first layer is deposited using a much higher WFS value of 8.89 m/min so that the penetration into the substrate is higher and thus there is no delamination.

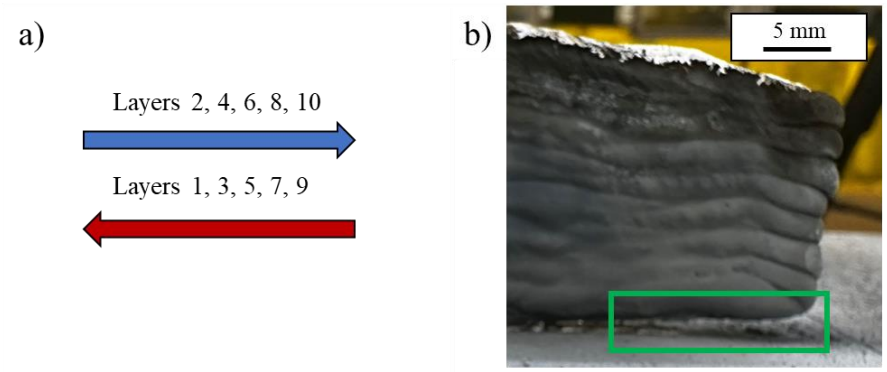

Figure 2: a) Path planning; b) delamination

The first stage of the experiments in this study is to experimentally determine the LED in J/mm of each parameter set by depositing a series of two bead walls, which consist of a preliminary high penetration bead and a subsequent bead using the experimental process parameter sets outlined in Table 2. After the LED has been experimentally determined using two bead builds, each parameter set is used to deposit single-bead, multi-layer walls consisting of 10 layers that are each 152.4 mm long.

C. Data Collection

Several process data streams are collected in-situ during the deposition process: the current, voltage, and power from the Fronius power supply, and the CTWD measurement extracted from the optical camera. The CTWD measurement is determined by finding the centroid of the welding arc, shown in the green box in Figure 3 below, and measuring that centroid distance from the contact-tip. The data from the Fronius power supply is sampled at approximately 10 Hz and the CTWD values are sampled from the optical camera at approximately 5 Hz.

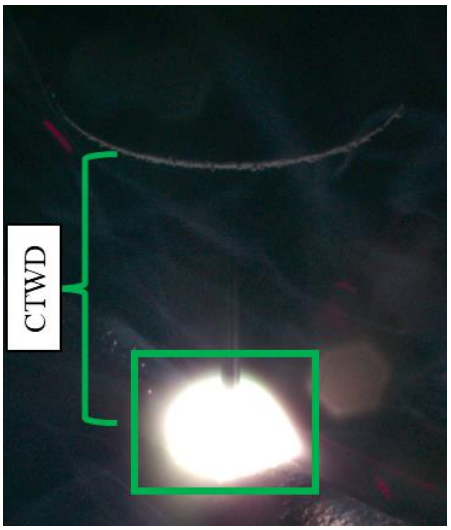

Figure 3: Example optical camera output

The geometry of the as-deposited parts is measured by using a Faro arm laser line scanner, which can capture point cloud data of the as-deposited part (Figure 4b) and create an STL file from that point cloud data (Figure 4c). Cross-section slices can then be extracted from the STL file and used to calculate the width of the as-deposited part at different part heights, as shown in Figure 4d below.

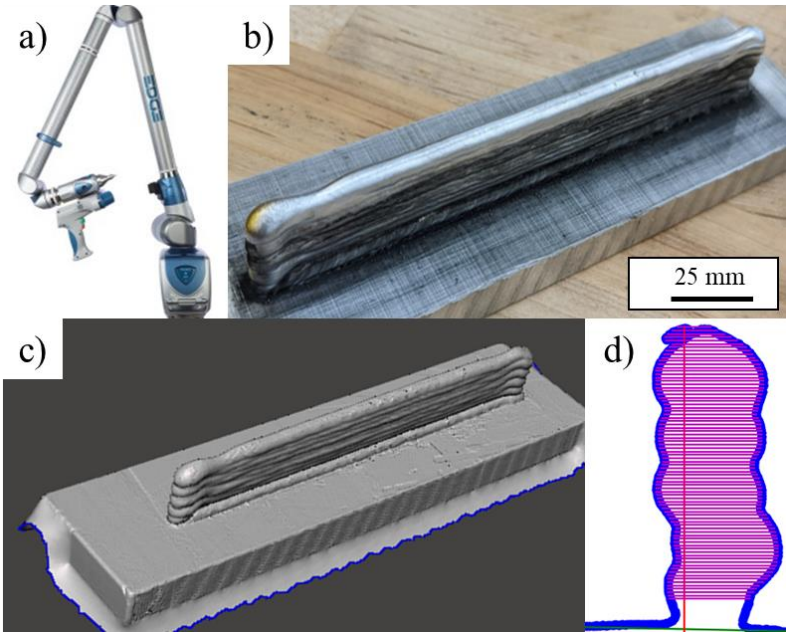

Figure 4: a) Faro arm scanner; b) as-deposited part; c) STL scan of as-deposited part; d) sample cross-section of STL showing part contour (blue) and extracted measurements (pink)

Radiography was conducted with a VisiConsult XRH222 with a 100 micron pixel pitch detector. The radiographs were taken at between 188-189 kV and 3.9-4 mA with 100 integrations. Due to size limitations of the radiography machine, only half of the sample was able to be captured at a time. A 1-2-3 block was used to calibrate the voxel size for analysis which was seen to be approximately 108 micron/voxel. Radiography images were then processed in Weka using the following options: Gaussian Blur, Hessian, membrane

projections, entropy, Sobel Filter, Difference of Gaussians, and median filters added to a fast random forest classifier. A porosity analysis was then conducted using Matlab's region properties analysis tool.

Results and discussion

A. 2-bead results

The LED for the second bead of each initial two bead build can be seen below in Figure 5. The LED increases from approximately 80 J/mm for experiments 1, 4, and 7 (which use TS, WFS values of 0.51, 4.7 m/min, respectively) to approximately 120 J/mm for experiments 2, 5, and 8 (which use TS, WFS values of 0.58, 5.33 m/min) and experiments 3, 6, and 9 (which use TS, WFS values of 0.66, 6.1 m/min). Each 2-bead experiment is only conducted once.

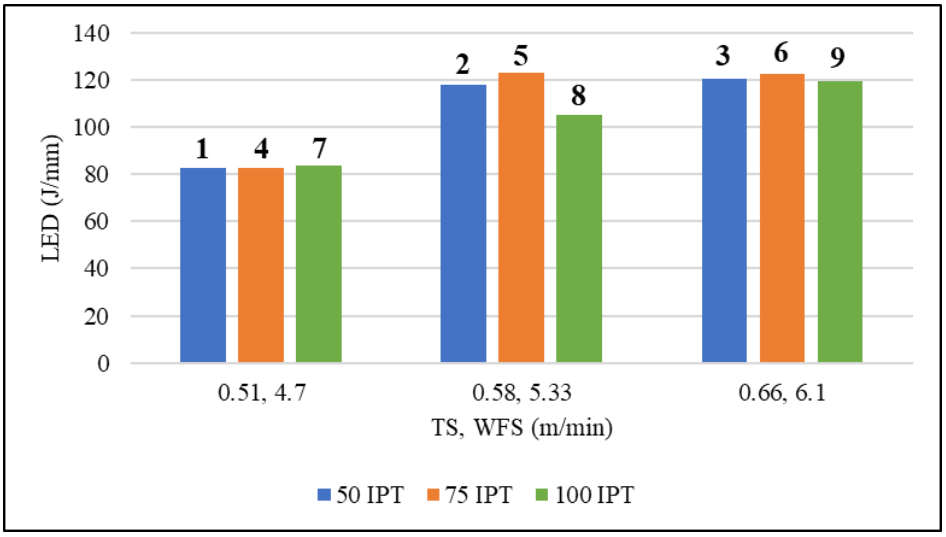

Figure 5: Variations in average linear energy density (LED) for each two-bead experiment, grouped by IPT. The experiment numbers are at the top of each bar, corresponding to Table 2.

B. 10-Layer Wall Preliminary Results

The as-deposited parts seen below in Figure 6 show that the part geometry remains stable as the TS, WFS, and IPT values are increased with the exception of the experiments 3, 6, and 9 where TS, WFS is set to 0.66, 6.1 m/min. In these experiments, the surface topology of the as-deposited components exhibits a large degree of waviness. This geometric disparity between the experiments occurs even though the WFS/TS ratio, and thus the material input rate, is approximately constant. Each wall part is only manufactured once.

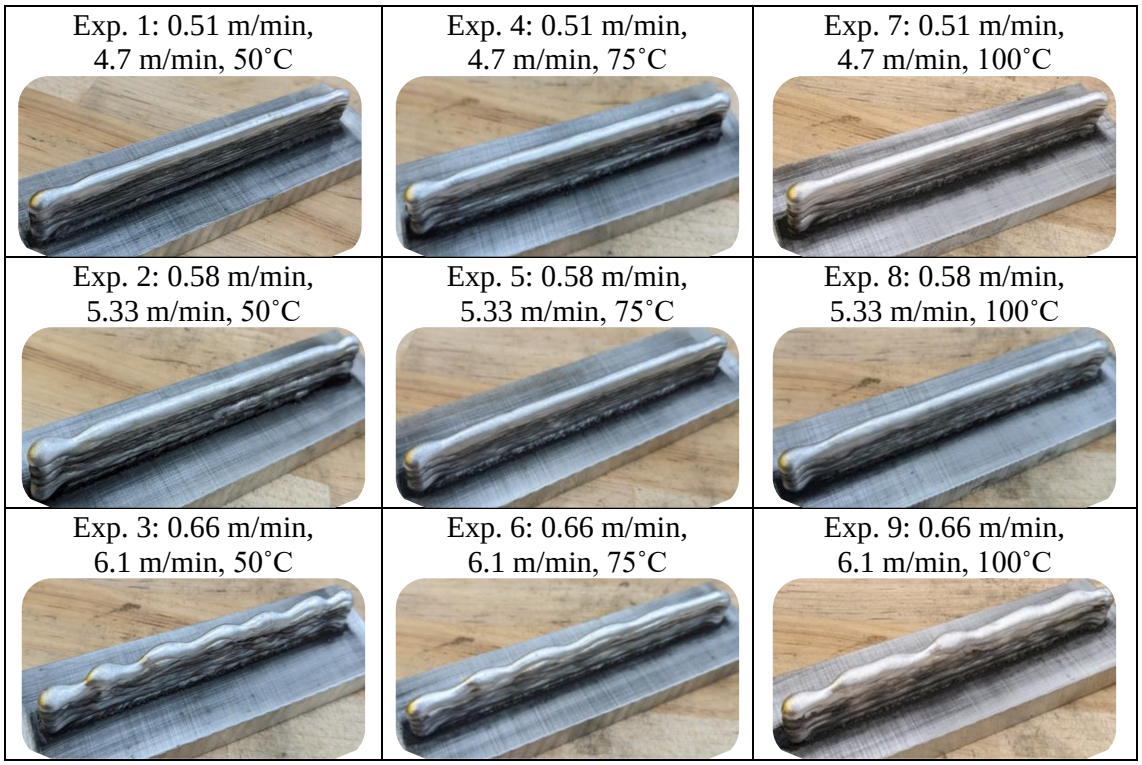

Figure 6: Images of each 10-layer wall constructed from the previous parameter set. The penetration bead again held the same parameters, while each additional layer was altered based on the experiment. The title of each image is based off experiment number and shows experiment parameters (TS, WFS, IPT).

C. 10-Layer Wall In-situ data Results

The variations of the in-situ process data streams of linear energy density (LED), current, voltage, power, actual WFS, and CTWD, can be seen below in Figure 7, where the average process condition values for each bead have been plotted. For all in-situ process data values except for CTWD, the average first bead values are much higher than those of the subsequent beads due to the high penetration process parameters used in the first bead to prevent delamination of the part from the substrate. It can also be seen that at the third bead of the deposition, the average current, power, and LED reach approximate steady state values of 70A, 975W, and 95 J/mm for the experiments 1, 4, and 7, and approximate steady state values of 80A, 1175W, and 110 J/mm for experiments 2, 5, and 8. The difference in current and power values can be explained by the different WFS values used. For experiments 3, 6, and 9, the average current, power, and LED values tend to fluctuate by approximately 15A, 400W, and 40 J/mm, respectively, but the grouping of these average values is distinctly separate from the steady state values of the other TS and WFS process parameter sets. The average voltage values seen in Figure 7b do not reveal any unique trends across the experimental parameter sets. For all the in-situ data streams taken from the Fronius power supply, the plotted data is grouped according to the TS, WFS values of the experimental process parameter set, indicating that the IPT is not an influential factor on the stability of the deposition process conditions.

The average CTWD values for the first bead range from 17-19 mm, and the subsequent average CTWD values follow a common trend of decreasing to approximately 16 mm for the second bead and then increasing for the subsequent beads. However, the average CTWD diverges depending on the experimental process parameter set. At the 10th bead, the average

CTWD for experiments 3, 6, and 9, which use TS, WFS combination of 0.66, 6.1 m/min, increases to approximately 19 mm, the average CTWD for experiments 2, 5, and 8, which use TS, WFS combination of 0.58, 5.33 m/min, increases to approximately 17 mm, and the average CTWD for experiments 1, 4, and 7, which use the TS, WFS combination of 0.51, 4.7 m/min, remains roughly level from approximately 15.5-16.5 mm. The larger increase in average CTWD for experiments 3, 6, and 9 can be explained by the surface topology waviness, which periodically increases the CTWD and thus, the average CTWD value. As with the other in-situ process data streams, the plotted CTWD data is grouped according to the TS, WFS values of the experimental process parameter set, indicating that the IPT is not an influential factor on the stability of the deposition process conditions.

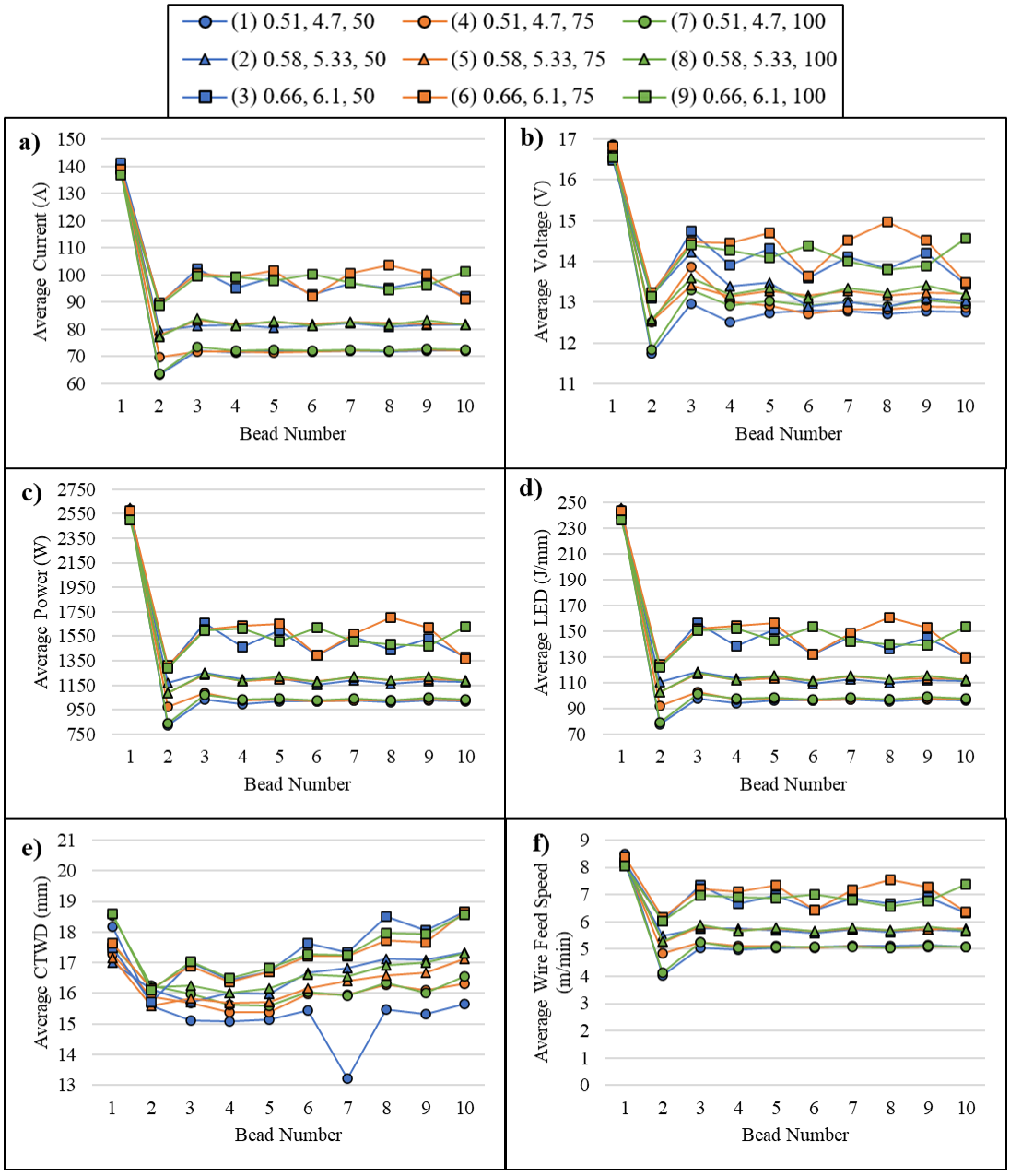

Figure 7: Variations of average parameters recorded for each bead deposited across each experiment. The parameters are a) current, b) voltage, c) power, d) LED, e) CTWD, and f) WFS. Experiment numbers are included in the legend at the top.

An analysis of the production time is also key to understanding the selection of optimal deposition parameters. In Figure 8a, the interpass dwell time for each bead can be seen. The most influential factor on the interpass dwell time is the IPT, which expected since it takes longer to cool to lower temperatures. The interpass dwell times for the experiments with 75 and 100 ºC IPT are somewhat similar and mostly range from approximately 100-200s whereas the interpass dwell times for the experiments with 50 ºC IPT range from approximately 200-450s. The overall deposition times (including both the time that the WAAM system is actively depositing material and the interpass dwell time) are seen in Figure 8b. These data reflect a similar trend to the data from Figure 8a, in that the experiments with 50 ºC IPT have the highest production times of approximately 2500-4000s, the experiments with 75 ºC IPT have higher production times (approximately 1000-1500s), and the experiments with 100 ºC IPT have production times of approximately 900-1100s. This indicates that varying the TS, which dictates the time needed to deposit material, is more influential on the production time at higher values of IPT. The increased cooling times seen in the first beads of experiments 1, 3, and 5 can be attributed to the combination of the high penetration process settings and low IPT value.

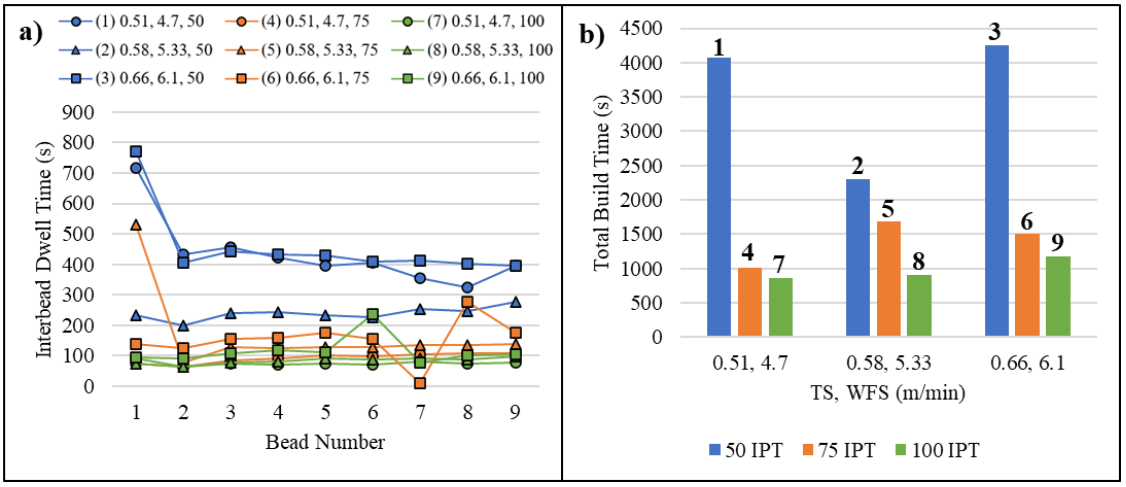

Figure 8: a) Interpass dwell time vs bead number for all process parameters. In the graph, each value refers to how long each bead took to cool down (for example, bead 1 in the 0.66-6.1-50 set took 772 seconds to cool to 50˚C, or 12:52 (in min:sec)). Bead 10 is excluded because there was no need to time the wait to the next bead deposition, as there is no bead 11. b) Total production time (dwell & deposition) for all process parameters.

D. 10-layer Wall Geometry Results

The as-deposited geometry is an important focal point of analysis as it can determine the viability of process parameters since the stochastic nature of geometry produced by additive manufacturing means that more stable as-deposited geometries are desired. Figure 9a below shows the part height profile from all experiments over the length of the part, where each height measurement is taken from individual 2D cross-section slices as shown previously in Figure 4. Similarly, Figure 9b shows the maximum part width from each 2D cross-section slice taken along the length of the part. The mean height and width values and their accompanying standard deviations can be seen in Figure 10 below.

The large degree of surface topology waviness from experiments 3, 6, and 9 can be readily seen in the height profile data and has a mean of approximately 22 mm, a standard deviation of approximately 1.5 mm, and ranges approximately 19 to 24 mm. Conversely, the height profiles of experiments 1, 4, and 7 can be seen to have much more consistent height

profiles with mean heights ranging from approximately 22.5-23.5 mm with standard deviations less than 1 mm. Experiments 2, 5, and 8 have mean heights ranging from approximately 21.5-22.5 mm with standard deviations ranging from 0.5 to 1.5 mm. The part width data shows similar trends, with the TS, WFS combination of 0.61, 6.1 m/min in experiments 3, 6, and 9 leading to more noticeable waviness, as compared to the other experimental parameter sets. This can be seen in the statistical data, as experiments 3, 6, and 9 have larger mean widths (ranging from approximately 6.5-7.5 mm), while the rest of the experiments have mean widths of approximately 5.5-6.5 mm. Although experiments 3, 6, and 9 have larger standard deviations in their part width, all standard deviations in the width measurements are less than 1 mm. Overall, it seems as though the IPT has little influence on the part geometry and that the main driver of part geometry quality is the TS, WFS combination.

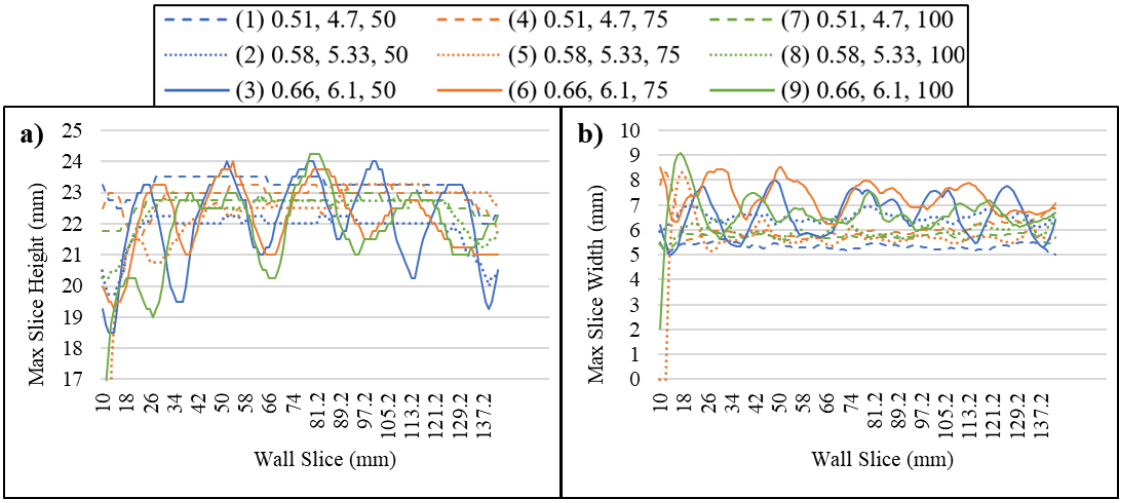

Figure 9: a) Maximum part height vs wall slice for all process parameters & b) Maximum part width vs wall slice for all process parameters

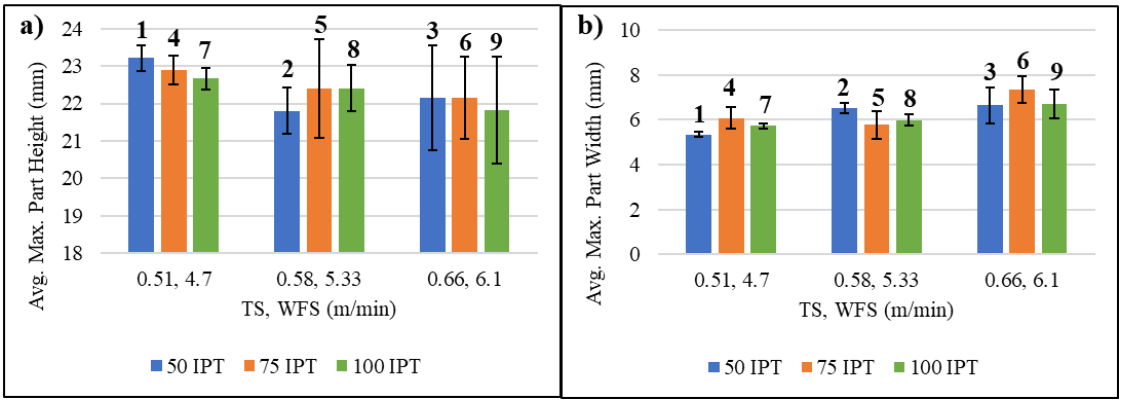

Figure 10: Graphical representations of variations in a) average maximum part height and b) average maximum part width for each 10-layer wall experiment.

E. 10-layer Wall X-Ray Results

Radiography results captured beam hardening effects in lower deposition layers. Figure 11 shows an example of a segmented porosity radiograph for experiment 4 (TS: 0.51 m/min, WFS: 4.7 m/min, IPT: 75 ºC). Due to the beam hardening, the authors restricted analysis to upper layers beyond the beam hardened region. Figure 12 shows the number of pores determined

from scans of both the left and right sides of each part. For an IPT of 100 ºC, the porosity is much lower across all combination of TS and WFS than in the 50 ºC cases, which have 7-45 pores, and in the 75 ºC IPT cases, which have 1-45 pores. The pore count on both the left and right sides of the TS, WFS combination of 0.51, 4.7 m/min is higher for the 75 ºC IPT case than the 50 ºC IPT case. The experiments using a TS, WFS combination of 0.58, 5.33 m/min appear to have no porosity after the first few layers for IPT conditions above 75 ºC and low pore counts at an IPT value of 75 ºC. Experiments 3, 6, 9, which use TS, WFS combination of 0.66, 6.1 m/min, had low amounts of porosity for all IPT values. Figure 13 shows the average equivalent diameter of the pores in millimeters. In general, the pores found in the study are very large (on the order of 100s of microns), indicating that they are lack of fusion pores and not gas pores.

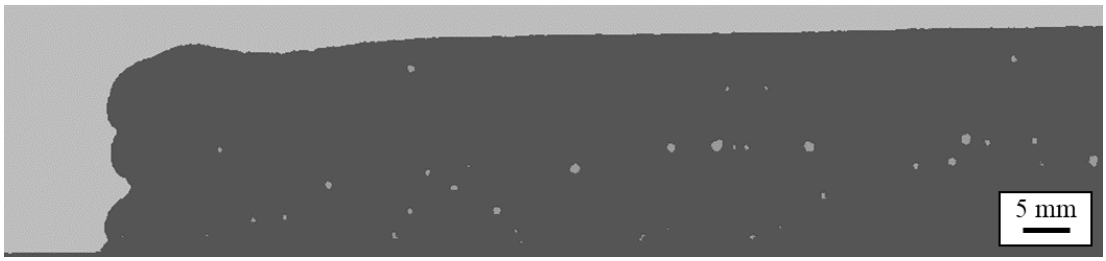

Figure 11: Sample segmented radiograph from TS: 0.51 m/min, WFS: 4.7 m/min, IPT: 75 ºC condition.

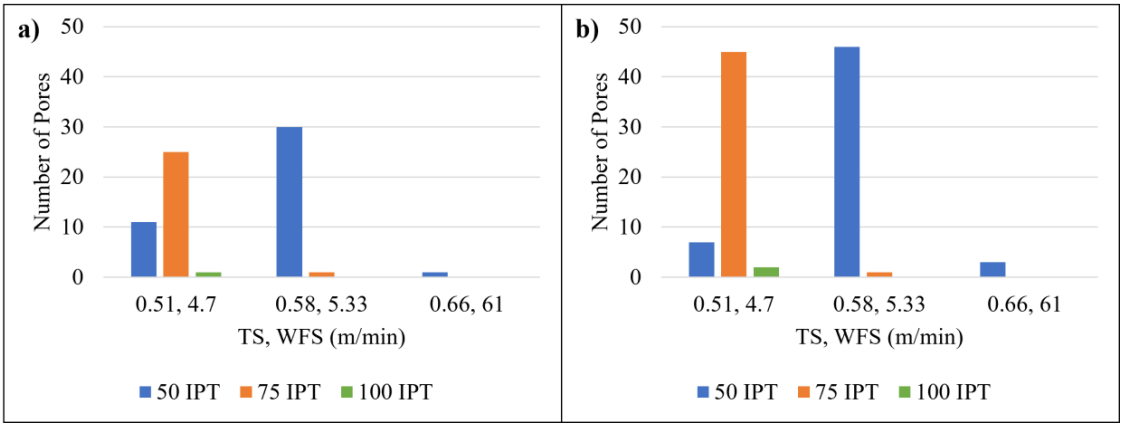

Figure 12: Count of pores on a) left side of the radiography scan b) right side of the radiography scan.

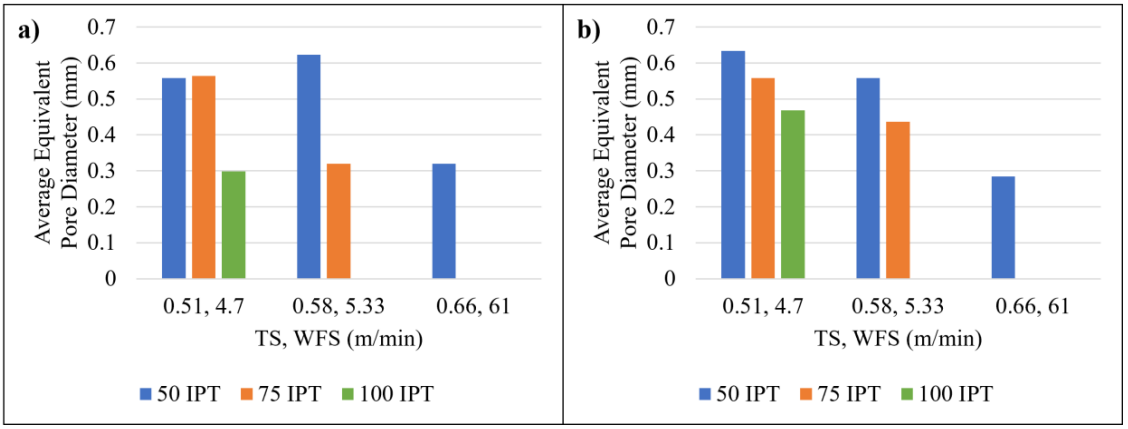

Figure 13: Average diameter on a) left side of radiograph b) right side of radiograph

Conclusion

In this study, the WAAM CMT process is utilized to fabricate several components with varying wire feed speed (WFS), traverse speed (TS), and interpass temperature (IPT) values in order to establish a viable process window that produces stable geometry and deposition conditions, while minimizing production times and porosity. Several in-situ process data streams are collected and analyzed for each experiment, along with measurement data to determine part geometry and digital X-ray radiographs to characterize any porosity. The results of this work have led to several import conclusions:

- The selection of WFS and TS dominates the resultant part geometry more than the IPT value, as experiments 3, 6, and 9, which have TS, WFS combinations of 0.66, 6.1 m/min, showed a high degree of surface waviness for across all IPT conditions. Therefore, a desirable process window for stable geometry dictates that the TS and WFS be kept below those values while maintaining the WFS/TS ratio.

- This surface waviness instability found in experiments 3, 6, and 9, which have TS, WFS values of 0.66, 6.1 m/min, can be reflected in the variation of the in-situ process data streams which indicates that these in-situ data streams could be useful for process monitoring and eventually closed loop control.

- The selection of the IPT value dictates the total production time for 50 ºC IPT, but incorporation of the active deposition time is critical to evaluating production time for the higher IPT values of 75 and 100 ºC.

- The porosity of the as-deposited part can be influenced by the TS, WFS, and IPT parameters. In general, a low IPT of 50 ºC induces porosity in the build and a high IPT of 100 ºC ensures little to no porosity in the build. However, porosity can be mitigated at low IPT values if a higher TS, WFS combination is used, albeit at the expense of geometric stability.

When considering geometric stability, production time, and porosity, the optimal set of process parameters is those of experiment 8 with a TS of 0.58 m/min, a WFS of 5.33 m/min, and an IPT of 100ºC.

Acknowledgments

This material is based on research sponsored by the U.S. Air Force under agreement number FA8650-22-2-2206. The U.S. Government is authorized to reproduce and distribute reprints for Governmental purposes notwithstanding any copyright notation thereon. The views and conclusions contained herein are those of the authors and should not be interpreted as necessarily representing the official policies or endorsements, either expressed or implied, or the U.S. Air Force or the U.S. Government.

References

[1] Rodrigues TA, Duarte V, Miranda RM, Santos TG, Oliveira JP. Current Status and Perspectives on Wire and Arc Additive Manufacturing (WAAM). *Materials*. 2019; 12(7):1121. https://doi.org/10.3390/ma12071121

[2] Knezović, N., Topić, A. (2019). Wire and Arc Additive Manufacturing (WAAM) – A New Advance in Manufacturing. In: Karabegović, I. (eds) New Technologies, Development and Application. NT 2018. Lecture Notes in Networks and Systems, vol 42. Springer, Cham. https://doi.org/10.1007/978-3-319-90893-9_7

[3] S. Selvi, A. Vishvaksenan, E. Rajasekar, Cold metal transfer (CMT) technology - An overview, Defence Technology, Volume 14, Issue 1, 2018, Pages 28-44, ISSN 2214-9147, https://doi.org/10.1016/j.dt.2017.08.002.

[4] K. S. Derekar (2018) A review of wire arc additive manufacturing and advances in wire arc additive manufacturing of aluminium, Materials Science and Technology, 34:8, 895-916, DOI: 10.1080/02670836.2018.1455012

[5] C. G. Pickin & K. Young (2006) Evaluation of cold metal transfer (CMT) process for welding aluminium alloy, Science and Technology of Welding and Joining, 11:5, 583-585, DOI: 10.1179/174329306X120886

[6] A. Horgar, H. Fostervoll, B. Nyhus, X. Ren, M. Eriksson, O.M. Akselsen, Additive manufacturing using WAAM with AA5183 wire, Journal of Materials Processing Technology, Volume 259, 2018, Pages 68-74, ISSN 0924-0136, https://doi.org/10.1016/j.jmatprotec.2018.04.014.

[7] E. Aldalur, A. Suárez, F. Veiga, Metal transfer modes for Wire Arc Additive Manufacturing Al-Mg alloys: Influence of heat input in microstructure and porosity, Journal of Materials Processing Technology, Volume 297, 2021, 117271, ISSN 0924-0136, https://doi.org/10.1016/j.jmatprotec.2021.117271.

[8] Klein, T., Schnall, M. Control of macro-/microstructure and mechanical properties of a wire-arc additive manufactured aluminum alloy. Int J Adv Manuf Technol 108, 235–244 (2020). https://doi.org/10.1007/s00170-020-05396-6

[9] Fang X, Zhang L, Chen G, Dang X, Huang K, Wang L, Lu B. Correlations between Microstructure Characteristics and Mechanical Properties in 5183 Aluminium Alloy Fabricated by Wire-Arc Additive Manufacturing with Different Arc Modes. Materials. 2018; 11(11):2075. https://doi.org/10.3390/ma11112075